PLOS ONE

Brain Imaging of Vesicular Monoamine Transporter Type 2 in Healthy Aging Subjects by 18F-FP-(+)-DTBZ PET

Kun-Ju Lin[1,2,3◗], Yi-Hsin Weng[2,4,5,6◗], Chia-Ju Hsieh[1,2], Wey-Yil Lin[4,5], Shiaw-Pyng Wey[1,2], Mei-Ping Kung[1,2,7], Tzu-Chen Yen[3], Chin-Song Lu[2,4,5,6]*, Ing-Tsung Hsiao[1,2,3]*

1 Department of Medical Imaging and Radiological Sciences, College of Medicine, Chang Gung University, Taoyuan, Taiwan, 2 Healthy Aging Research Center, Chang Gung University, Taoyuan, Taiwan, 3 Department of Nuclear Medicine and Molecular Imaging Center, Chang Gung Memorial Hospital, Taoyuan, Taiwan, 4 Division of Movement Disorders, Department of Neurology, Chang Gung Memorial Hospital, Taoyuan, Taiwan, 5 Neuroscience Research Center, Chang Gung Memorial Hospital, Taoyuan, Taiwan, 6 School of Medicine, Chang Gung University, Taoyuan, Taiwan, 7 Department of Radiology, University of Pennsylvania, Philadelphia, Pennsylvania, United States of America

Abstract

18F-FP-(+)-DTBZ is a novel PET radiotracer targeting vesicular monoamine transporter type 2 (VMAT2). The goal was to explore the image features in normal human brains with 18F-FP-(+)-DTBZ as a reference of molecular landmark for clinical diagnosis in Parkinson's disease (PD) and related disorders.

Materials and Methods: A total of 22 healthy subjects (59.3 ± 6.0 years old) including 7 men and 15 women were recruited for MRI and 18F-FP-(+)-DTBZ PET scans. A total number of 55 brain VOIs were selected for quantitation analysis. The regional specific uptake ratio (SUR) was calculated with occipital as reference from MRI-based spatially normalized 18F-FP-(+)-DTBZ images. Regional percentage SUR to that of anterior putamen was calculated. Average SUR images were displayed in 2D and 3D space to illustrate the image patterns. The correlation between age and regional VMAT2 uptake was also examined.

Results: Visual assessment showed symmetric uptake of 18F-FP-(+)-DTBZ and obviously highest in striatum, followed by nucleus accumbens, hypothalamus, substantia nigra, and raphe nuclei. Quantification analysis revealed striatal VMAT2 density of anterior putamen>posterior putamen>caudate nucleus. Other subcortical regions were with moderate VMAT2 distribution (6~51% SUR of anterior putamen), while slightly lower VMAT2 was observed in cerebellum (10.60% SUR) and much lower in neocortex (<5% SUR). No significant correlation of SUR to age was found in subcortical regions.

Conclusion: Using 18F-FP-(+)-DTBZ PET, we showed the 2D and 3D imaging features of the VMAT2 distribution *in vivo* in healthy aging brains. The *in vivo* imaging characteristics of VMAT2 is consistent with the expression of VMAT2 in a recent autopsy study. Therefore, 3D visualization and higher image quality of 18F-FP-(+)-DTBZ PET imaging might potentially be a powerful biomarker in detecting VMAT2 distribution of subcortical regions, and for Parkinson's disease and related neuropsychiatric disorders involving related monoaminergic systems.

Introduction

The type 2 vesicular monoamine transporter (VMAT2) is a protein responsible for pumping monoamine neurotransmitters, including dopamine (DA), norepinephrine (NE) and serotonin (SE), from the neuronal cytosol into synaptic vesicles. Measurement of the VMAT2 density in brain can serve as a diagnosis tool for many neuropsychiatric diseases related to monoaminergic dysfunction. Since more than 90% of VMAT2 locate in the dopamine nerve terminals [1], the *in vivo* estimation of VMAT2 density may have great help for the diagnosis and management of disorders associated with nigrostriatal degeneration, such as

Parkinson's disease (PD). In previous studies, positron emission tomography (PET) imaging with the VMAT2 tracer 11C-dihydrotetrabenazine (11C-DTBZ) has been proven to be an objective marker of nigrostriatal terminal integrity [2].

A novel tracer 18F-9-fluoropropyl-(+)-dihydrotetrabenzazine (18F-FP-(+)-DTBZ) for VMAT2 imaging with a longer half-life ($t_{1/2} = 110$ min) has been recently developed [3]. 18F-FP-(+)-DTBZ PET imaging has a high sensitivity for detecting dopaminergic integrity in both healthy subjects and PD patients [4,5,6]. Yet the detailed imaging characteristics of VMAT2 distribution in healthy aging human brains with 18F-FP-(+)-DTBZ PET have not been well described.

PD is a neurodegenerative disorder characterized by a clinical spectrum of motor and non-motor disabilities. The major pathological feature is the degeneration of DA neurons in the substantia nigra (SN) and axons projecting to the striatum [7]. In addition to the nigrostriatal DA system, the mesocortical/meolimibic pathways and those involving the NE and SE systems also play important roles in the neuropsychiatric symptoms and prognosis of PD [8,9,10,11]. Thus, to study the *in vivo* VMAT2 distribution in the whole brain, particularly in the extrastriatal regions, is very important for further clinical applications, and for exploration of extended diagnostic utility of the novel tracer.

Following recent advances in the resolution and sensitivity of PET, the goal of this study is to establish the imaging features of the ^{18}F-FP-(+)-DTBZ for normal VMAT2 distribution, and establish a normal basis for future diagnostic comparison in VMAT2 imaging studies. In particular, the 2D (two-dimension) and 3D (three-dimension) distribution patterns of VMAT2 binding within the dopamine pathways in normal aging brain were further investigated for a better visual analysis. In addition, the quantification on VMAT2 binding was also measured and compared between different brain regions of dopaminergic systems. All the obtained imaging data were compared with the results from previous in vitro studies [12,13,14].

Materials and Methods

Subjects

A total of 22 healthy subjects including 7 men and 15 women with age 59.3±6.0 years (range: 52–71 year) were enrolled. The study protocol was approved by the Institutional Review Board of the Chang Gung Memorial Hospital and the Food and Drug Administration, Taiwan, and a written informed consent was obtained prior to all procedures for each participant. Healthy subjects had no evidence of significant neurodegenerative disease by history and neurologic testing, and no clinically significant or unstable medical or psychiatric illness, and neither any documented abnormality in the MRI of brain.

Data Acquisition

^{18}F-FP-(+)-DTBZ was prepared at the cyclotron facility of Chang Gung Memorial Hospital as described previously [15]. PET scans were performed for all subjects in a Biograph mCT PET/CT System (Siemens Medical Solutions, Malvern, PA, USA) with a 3-dimentional acquisition mode. In addition, all subjects underwent magnetic resonance imaging (MRI) on a 3T Siemens Magnetom TIM Trio scanner (Siemens Medical Solutions, Malvern, PA, USA) for screening of other diseases, obtaining structural information, generating volumes of interest (VOIs), and performing spatial normalization with PET images.

After injection of 383±14 MBq ^{18}F-FP-(+)-DTBZ, a single 10-min PET scan was acquired 90 min post injection in 3D mode [5]. PET images were then reconstructed using 3D OSEM algorithm (4 iterations, 24 subsets; Gaussian filter: 2 mm; zoom: 3) with CT-based attenuation correction, and also scatter and random correction as provided by the manufacture. The reconstructed images were with a matrix size of 400×400×148 and a voxel size of 0.68×0.68×1.5 mm^3.

Image Analysis

All image data were processed and analyzed using PMOD image analysis software (version 3.3, PMOD Technologies Ltd, Zurich, Switzerland). The 3D visualization of the VMAT2 distribution was processed and displayed as overlaid with the corresponding nigrostriatal VOIs using the AVIZO software (version 7, VSG Company, Germany). Each PET image was co-registered to the corresponding MR image, and the individual MR image was spatially normalized to the Montreal Neurological Institute (MNI) MRI template [16]. The spatial normalization parameters were then applied to PET images to form a final, spatially normalized PET image in the MNI domain. A total number of 58 VOIs within subcortex, neocortex, cingulum, and cerebellum were defined on the MNI template for later analysis. Nineteen subcortical VOIs were delineated on the MNI MRI template manually including bilateral caudate nuclei, anterior/posterior putamen, nucleus accumbens (NAc), substantial nigra (SN), raphe nuclei, locus coeruleus, brain stem, hypothalamus, amygdala, hippocampus, parahippocampus, and thalamus. In addition, a total number of 36 VOIs of neocortex, cingulum, and cerebellum were defined on the AAL VOI template for later analysis [17] (including vermis, bilateral anterior cingulum, middle cingulum, posterior cingulum, motor area, middle frontal, inferior frontal, medial frontal, superior parietal, inferior parietal, superior temporal, middle temporal, inferior temporal, superior occipital, middle occipital, and inferior occipital regions). The specific uptake ratio (SUR) for each VOI was calculated as [(uptake in target VOI-uptake in reference VOI)/uptake in reference VOI] [18] to reflect an estimate for the specific binding in different regions. The inferior occipital cortex was applied as the reference region [5]. The mean values from bilateral subcortical, neocortical, cingulate, and cerebellar VOIs were calculated for distribution comparison. In addition, a percentage SUR was also calculated as the normalized VMAT2 levels to the structure with the highest uptake [12].

Statistical Analysis

The difference between left and right sides regional SUR was statistically compared using the nonparametric Mann-Whitney test, and the percent difference was also calculated for left and right sides comparison. The correlation between age and VMAT2 uptake level was examined for each VOI using Spearman's correlation coefficient. P value of 0.05 was defined as the threshold of statistical significance in all tests.

Results

The average ^{18}F-FP-(+)-DTBZ 2D and 3D SUR images from 22 healthy subjects are illustrated in Figure 1. The sagittal view of the PET images in the section of right SN was displayed in Figure 1A. The uptake of ^{18}F-FP-(+)-DTBZ was obviously high in hypothalamus, SN, and raphe nuclei, and slightly increased in cerebellum. There was almost no visible distribution of ^{18}F-FP-(+)-DTBZ in the cortex. In Figure 1A, the three lines indicate three different 2D transverse views as illustrated in Figure 1B, 1C and 1D at the level of striatum, NAc, and brain stem, respectively. The uptake of ^{18}F-FP-(+)-DTBZ was symmetric and obviously the highest in striatum, followed by NAc, hypothalamus, SN, raphe nuclei, locus coeruleus, brain stem, amygdala and hippocampus. The caudate and putamen were well defined and could be easily differentiated from each other in the PET image without coregistration of MRI. The VMAT2 density was much lower in all cortical regions, whereas the uptake of ^{18}F-FP-(+)-DTBZ in cerebellum was higher and similar to those of hippocampus, thalamus and amygdala. Furthermore, we illustrated the VMAT2 density as a 3-D picture for the major VMAT2 systems (Figure 1E) at the posterior (Figure 1F), right lateral (Figure 1G), and anterior (Figure 1H) views. In addition, a movie is shown in the supporting Figure S1 to illustrate the 3D visualization of subcortical VMAT2 binding in different angles. This revealed an integral and visible
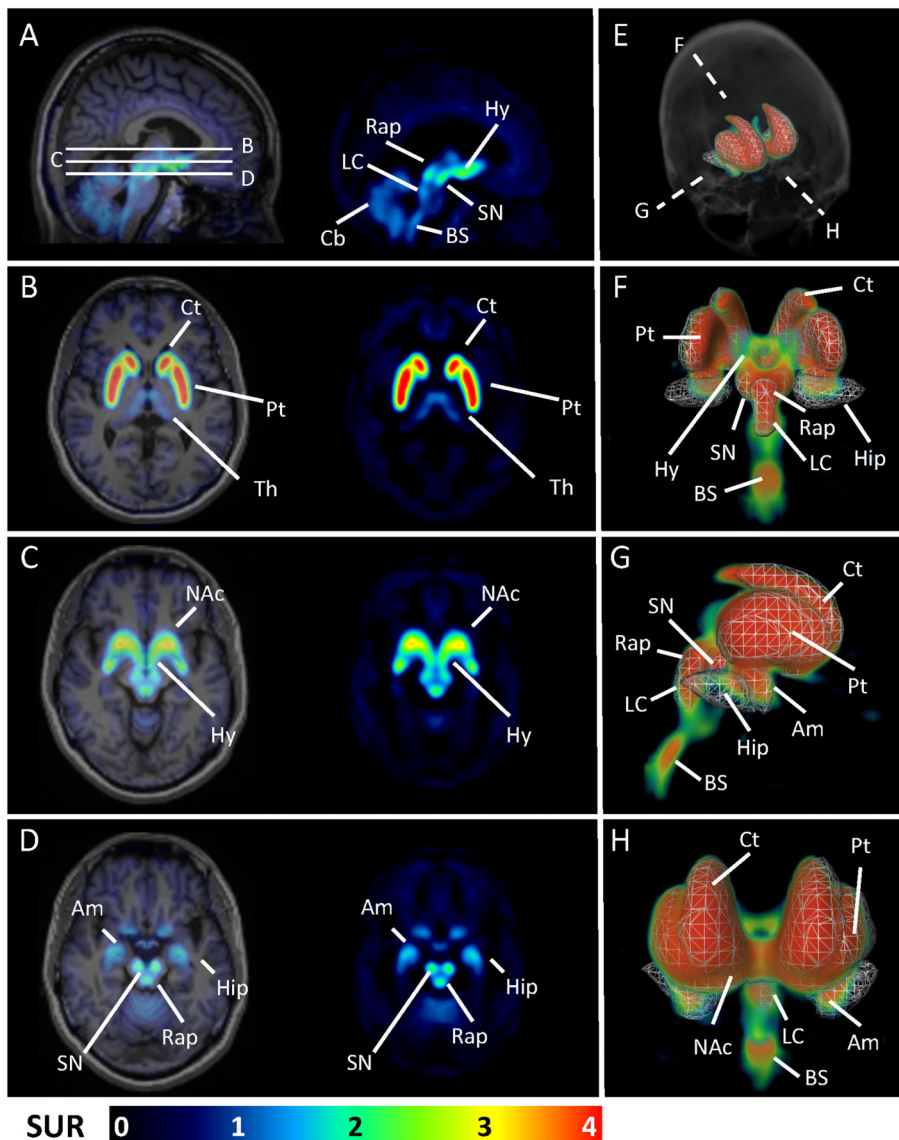
Figure 1. 2D and 3D views of the average VMAT2 distribution in normal aging brain using ^{18}F-FP(+)-DTBZ. The sagittal view of the VMAT2 distribution in the section of right substantia nigra was displayed in (A) with the three lines indicating three different 2D transverse views as illustrated in (B), (C) and (D) at the level of striatum, NAc, and brain stem, respectively. The 3D visualizations of subcortical VMAT2 binding were illustrated in (E) and also at the views of (F) posterior, (G) right lateral, and (H) anterior with corresponding VOI.
doi:10.1371/journal.pone.0075952.g001

functional anatomy of dopaminergic, serotoninergic, and norepinephrinergic innervations with clear spatial correlation in 3D space.

Table 1 shows the mean SUR from 58 VOIs divided into 4 groups including subcortical, cerebellum, cingulate, and neocortex. There was no significant SUR difference between left and right sides of each region (p value<0.05). The average and standard deviation of SUR in all regions were shown in the first column of Table 1. The uptakes of ^{18}F-FP-(+)-DTBZ were the highest in the anterior putamen (SUR = 2.78), followed by posterior putamen (2.68) and caudate (2.27). For each region, the percentage of regional SUR to that of the anterior putamen was also calculated and shown in the second column of Table 1. The VMAT2 density in the SN (SUR = 1.08) was about 38.75% of striatal SUR. Other high uptake ratios in the subcortical regions were observed in NAc (1.43), hypothalamus (1.29), raphe nuclei

(1.06), and locus coeruleus (1.00). The VMAT2 activity was slightly higher in brain stem (0.72), hippocampus (0.24), amygdala (0.47), and thalamus (0.18). All of the neocortical areas had low ^{18}F-FP-(+)-DTBZ uptakes that were less than 5% of uptake in the anterior putamen. The VMAT2 density in cerebellum (10.60% SUR) was slightly higher than that in neocortex. In addition, the uptake value in anterior putamen was three-fold higher than those of cerebellum and neocortex. Furthermore, no significant correlation of regional SURs to age was found in subcortical regions, but with a trend of decline. To make the data publicly available, Table S1 showed the regional SURs from each subject in this study.

Figure 2 displays the mean SUR value and percentage of regional SURs normalized to that of anterior putamen. According to the main types of monoaminergic axons/neurons and functional pathways in these brain areas, the regional SURs could

Table 1. Regional mean VMAT2 uptake.

	Regions	Average left and right sides	SUR Normalize to Anterior Putamen(%)	Left side	Right side	p value[a]
Subcortex	Caudate	2.27±0.43	81.50	2.22±0.44	2.31±0.43	0.4812
	Anterior Putamen	2.78±0.48	100.00	2.79±0.45	2.77±0.51	0.5973
	Posterior Putamen	2.68±0.48	96.46	2.72±0.54	2.64±0.44	0.8053
	Substantia Nigra	1.08±0.25	38.75	1.09±0.27	1.06±0.23	0.7336
	Nucleus Accumbens	1.43±0.59	51.41	1.41±0.53	1.45±0.68	0.9626
	Raphe nuclei	1.06±0.18	37.94			
	Hippocampus	0.24±0.07	8.47	0.25±0.08	0.23±±0.07	0.4449
	Amygdala	0.47±0.13	16.84	0.48±0.13	0.46±0.13	0.8694
	Hypothalamus	1.29±0.20	46.47	1.30±0.22	1.28±0.21	0.7599
	Thalamus	0.18±0.09	6.30	0.18±0.09	0.17±0.09	0.9065
	Locus coeruleus	1.00±0.14	35.90			
	Brain Stem	0.72±0.13	25.96			
Cerebellum	Vermis	0.21±0.09	7.51			
	Cerebellum Cortex	0.29±0.09	10.60	0.27±0.09	0.32±0.08	0.1126
Cingulate	Anterior Cingulum	0.11±0.10	3.78	0.11±0.11	0.10±0.11	0.7600
	Middle Cingulum	0.11±0.08	4.05	0.12±0.08	0.11±0.09	0.6294
	Posterior Cingulum	0.07±0.10	2.40	0.07±0.11	0.06±0.10	0.4174
Neocortex	Superior Frontal	0.09±0.05	3.10	0.09±0.05	0.09±0.06	0.9812
	Middle Frontal	0.08±0.05	3.01	0.08±0.05	0.09±0.06	0.8780
	Inferior Frontal	0.01±0.05	0.39	0.01±0.05	0.01±0.05	0.7240
	Medial Frontal	0.07±0.06	2.63	0.07±0.06	0.08±0.07	0.5250
	Motor Area	0.01±0.05	0.32	0.00±0.06	0.02±0.05	0.5883
	Superior Parietal	−0.04±0.06	−1.48	−0.02±0.06	−0.06±0.06	0.0651
	Inferior Parietal	0.01±0.04	0.36	0.01±0.04	0.01±0.04	0.8782
	Superior Temporal	0.00±0.06	0.00	−0.04±0.07	−0.03±0.08	0.6892
	Middle Temporal	0.08±0.05	2.84	0.08±0.05	0.08±0.05	0.8687
	Inferior Temporal	0.08±0.03	2.99	0.08±0.03	0.08±0.04	0.5545
	Superior Occipital	−0.03±0.04	−1.19	−0.04±0.04	−0.02±0.04	0.0896
	Middle Occipital	0.01±0.03	0.53	0.01±0.03	0.02±0.04	0.8408
	Inferior Occipital	-	-	0.01±0.03	−0.01±0.03	0.0706

[a]difference between left and right side.
The regional mean SURs were divided into 4 groups of subcortex, cerebellum, cingulate, and neocortex. Percentage SURs normalized to that of anterior putamen and P-value of bilateral difference were also shown.
doi:10.1371/journal.pone.0075952.t001

be further divided into several parts: the nigrostriatal (DA), mesolimbic (DA), NE, SE and mixed pathways. Caudate and putamen innervated by DA neurons of SN had the highest SURs. In addition to the nigrostriatal pathway, NAc, the major relay nucleus of mesolimbic system receiving the DA projections from ventral tegmentum area (VTA), had the second highest SUR of the whole brain (51.4%). Hypothalamus innervated by both serotonin and norepinephrine axons also had high VMAT2 density (46.5%). Moreover, the VMAT2 uptake in locus coeruleus innervating pure norepinephrine axons was slightly lower than hypothalamus (35.9%). In the serotonin system, the highest uptake of 18F-FP-(+)-DTBZ was found in the raphe nucleus (37.9%). In the limbic system, the binding of 18F-FP-(+)-DTBZ was the highest in amygdala followed by hippocampus with SURs of 16.8% and 8.5%, respectively. The uptakes of 18F-FP-(+)-DTBZ were much lower in all cortical regions (<5%). The SUR of cerebellar cortex was higher than those of neocortex (10.6%).

Discussion

The present study provided the distribution of VMAT2 in healthy aging brains by 2D and 3D 18F-FP-(+)DTBZ PET imaging (Figure 1). The brain structures with high VMAT2 density, including striatum, SN, raphe nuclei, NAc and limbic system, were clearly illustrated by 18F-FP-(+)-DTBZ PET imaging. In particular, the 3D images of 18F-FP-(+)-DTBZ PET demonstrated the anatomical relationship more precisely than the 2D images between the brain structures. The 3D images could help physicians and researchers to recognize the different VMAT2 distribution in individual case. With this, the usefulness of 18F-FP-(+)-DTBZ in detecting the disease-related alteration of VMAT2 density by visual assessment should be expected. Ultimately, the diagnostic accuracy in many neuropsychiatric disorders, such as PD and depression could be improved.

Recently, Tong et al. showed VMAT2 protein distribution in autopsied normal human brain by quantitative immunoblotting
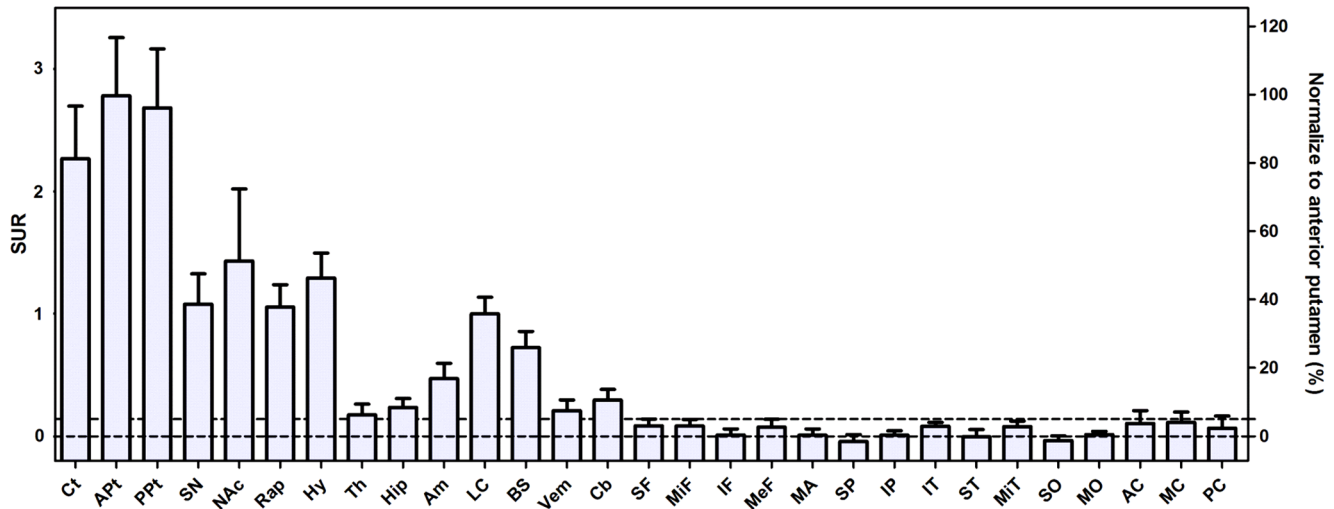
Figure 2. The mean regional SUR value and percentage SUR normalized to that of anterior putamen. Two dash lines indicated levels of 0% (lower) and 5% (upper) SUR to the anterior putamen, respectively. This clearly illustrated the distribution spectrum of VMAT2 density in the regions of subcortex, cerebellum, cingulate and neocortex. Ct: Caudate, APt: Anterior Putamen, PPt: Posterior Putamen, SN: Substantia nigra, NAc: Nucleus accumbens, Rap: Raphe, Hy: Hypothalamus, Th: Thalamus, Hip: Hippocampus, Am: Amygdala, LC: Locus coeruleus, BS: Brain stem, Vem: Vermis, Cb: cerebellum cortex, SF: Superior Frontal, MiF: Middle Frontal, IF: Inferior Frontal, MeF: Medial Frontal, MA: Motor Area, Olf: Olfactory, SP: Superior Parietal, IP: Inferior Parietal, ST: Superior Temporal, MiT: Middle Temporal, IT: Inferior Temporal, SO: Superior Occipital, MO: Middle Occipital, AC: Anterior Cingulate, MC: Middle Cingulate, PC: Posterior Cingulate.
doi:10.1371/journal.pone.0075952.g002

[12]. They concluded that the VMAT2 protein was the highest in putamen, followed by caudate, SN, hypothalamus and red nucleus. The cerebellar and cerebral cortices contain negligible VMAT2 protein versus the striatum. In the present study, the quantification analysis showed that the VMAT2 level was the highest in the putamen and caudate (the nigrostriatal pathway), followed by NAc (mesolimbic system) and hypothalamus. Low uptakes of ^{18}F-FP-(+)-DTBZ were observed in cortex and cerebellum. Our results showed that the ratios of regional SURs normalized to that of the anterior putamen displayed similar pattern to the expression of VMAT2 protein obtained from autopsied human brains [12,19]. Furthermore, the SURs in SN and raphe nuclei were approximately 60%∼70% lower than that in putamen for normal brains. This finding was also similar to the postmortem study that the densities of VMAT2 in SN and midbrain were about 20%∼30% of that in putamen for healthy controls [12]. It is noted that the VMAT2 level in raphe nuclei is mainly due to serotonergic innervation. In addition, as compared to the SUR in caudate, higher ^{18}F-FP-(+)-DTBZ binding was observed in both anterior and posterior putamen but with no statistically significant difference (p = 0.6220) between these two putaminal VOIs in our study. The different VMAT2 distribution between caudate and putamen observed in the autopsied result [12], as well as previous in vivo ^{18}F-FP-(+)-DTBZ and ^{11}C-DTBZ studies [4,5,20], suggested a slightly lower density of VMAT2 in caudate than in putamen. Similar result of insignificant difference was found in the ^{11}C-DTBZ study but with slightly lower uptake level in anterior putamen than posterior putamen [20]. Similar to the data in a recent report [14], our study also showed a relatively lower VMAT2 density in the NAc as compared to both caudate and putamen in normal brains.

The degeneration of dopamine neurons is not only confined to the nigrostriatal pathway for patients with early PD. For example, a recent FDOPA study reported additional degeneration in motor and anterior cingulate cortices [21]. Therefore, the capability of

quantification for VMAT2 level in the extrastriatal regions might provide more information for studying non-motor symptoms in PD [21]. However, the previous in vivo and in vitro studies [12,22,23] reported low specific VMAT2 binding in the cortex. Another in vivo study also suggested that the cortical VMAT2 binding was too low to be reliably quantified using (+)-stereoisomer of ^{11}C-DTBZ [20]. Consistently, our study indicated lower neocortical VMAT2 density (<5% SUR of anterior putamen) and thus being challenging for further quantification study in these regions. Nevertheless, many regions of the monoaminergic system, including NAc, amygdala, hypothalamus, raphe, and even thalamus and hippocampus, contain sufficient VMAT2 density to be quantifiable. Our results showed that ^{18}F-FP-(+)-DTBZ PET imaging could detect the monoaminergic integrity in these extrastriatal regions. It suggested that ^{18}F-FP-(+)-DTBZ PET might be a useful imaging biomarkers, not only for PD, but also for other neuropsychiatric disorders, such as affective disorders and schizophrenia.

The measurement of the ^{18}F-FP-(+)-DTBZ uptake in this study was based on a semiquantitation method [5,24]. The usual standard uptake value ratio (SUVR) was measured as an alternative estimate of the distribution volume ratio (DVR) which indicates distribution ratio of total ligand binding to the displaceable ligand amount [25]. Then SUR (specific uptake ratio = SUVR-1.0) was calculated as an estimate for amount of specific binding in brain imaging [18,26] to provide a more informative interpretation of the VMAT2 binding. Here, occipital cortex was used as the reference region since it was found with very low VMAT2 expression as reported by in vitro studies [12,19]. Some earlier studies applied cerebellum as a reference region but more consistent and higher binding values were observed when occipital region was used as the reference [27]. Similar to previous studies [20,27,28], our study also displayed a relatively higher SUR in the cerebellum and this might again explain why the lower binding values in the targets resulted from

using cerebellum as the reference region. Therefore, the same distribution pattern but lower SUR values than those from the reference region of occipital cortex can be obtained when using cerebellum as the reference region. The measures based on using the occipital cortex as the reference region was reported with higher reliability than that from cerebellum in a test-retest study of ^{11}C-DTBZ [27]. Other than occipital cortex and cerebellum, white matter might be considered as a reference region. However, heterogeneous distribution of free and nonspecific binding and difficulty in consistent region delineation for white matter are two main challenges [20]. Further study is necessary to investigate these effects for ^{18}F-FP-(+)-DTBZ. Nevertheless, a similar amount of VMAT2 proteins in both cerebellum and occipital was reported from an in vitro study [12]. The discrepancy that imaging study showed relatively higher in vivo VMAT2 binding in cerebellum as compared to occipital might be due to protein availability between in vivo and in vitro, and possible partial volume effect in PET imaging [12] caused by the relatively small size of cortical regions. For the later reason, future work should include partial volume correction to improve the quantitation and to study this discrepancy.

Our study showed no significant aging-related decline in the nigrostriatal system, brain stem, hypothalamus, amygdala and hippocampus. The result of no significant correlation of VMAT2 density in the nigrostriatal pathway with age change was consistent with the in vitro [12,29] and in vivo PET studies [27,30]. On the contrary, the age-related decline of dopamine transporters (DAT) is well documented [26,31,32,33,34]. In addition, some in vivo VMAT2 studies using ^{11}C-DTBZ also reported normal nigrostriatal aging effect [31,35]. Our study suggested that VMAT2 was a relatively stable target during aging process. Age might not be an important confounding factor in the interpretation of ^{18}F-FP-(+)-DTBZ PET images. Therefore, unlike DAT imaging, to "compare age-matched controls" may not be so critical for the ^{18}F-FP-(+)-DTBZ PET studies for diseases involving the nigrostriatal system, at least for the population aged more than 50 years [26]. However, the aging effect of the ^{18}F-FP-(+)-DTBZ binding in a younger population cannot be overlooked and needs further study.

Three-dimensional volume visualization has already demonstrated improvement in clinical care and diagnosis power for many imaging applications [36,37,38]. Due to the availability of a PET scanner with higher resolution and sensitivity, our study displayed a clear 3D visualization of in vivo VMAT2 binding in various brain structures. The use of 3D visualization for VMAT2 distribution might add additional diagnostic power in VMAT2 imaging studies, and deserves further studies to explore potential diagnostic applications. Future work should also include a test-retest reliability analysis before applying this tracer for use in general clinical diagnosis.

Conclusion

This work provided 2D and 3D imaging features of the *in vivo* VMAT2 distribution in the healthy aging human brains using ^{18}F-FP-(+)-DTBZ PET imaging. The VMAT2 distribution pattern was not only explored in the usual nigrostriatal pathways, but also the mesolimbic and mesocortical pathways, serotonin and norepinephrine pathways. The *in vivo* imaging characteristics of VMAT2 displayed similar distribution patterns to the *in vitro* VMAT2 protein levels reported in a recent autopsy study. We concluded that 3D visualization and higher image quality of ^{18}F-FP-(+)-DTBZ PET imaging can improve diagnosis power for VMAT2 studies. The capability of ^{18}F-FP-(+)-DTBZ PET in detecting VMAT2 of subcortical regions may help in clinical evaluation of many neuropsychiatric disorders that involved these monoaminergic systems.

Supporting Information

Figure S1 The 3D views of the average VMAT2 distribution in normal aging brain using ^{18}F-FP(+)-DTBZ. This illustrates the 3D visualization of subcortical VMAT2 binding in different angles. The image was displayed and overlaied on a corresponding CT image.
(MPG)

Table S1 Regional SUR for each subject. The regional SURs from each subject were listed and divided into 4 groups of subcortex, cerebellum, cingulate, and neocortex. SUR from bilateral regions were averaged. Please see Fig. 2 for acronyms used in this table.
(DOCX)

Acknowledgments

Author Contributions

Conceived and designed the experiments: KJL YHW CSL TCY ITH. Performed the experiments: KJL YHW CJH WYL SPW. Analyzed the data: KJL YHW CJH WYL CSL ITH. Contributed reagents/materials/analysis tools: YHW MPK TCY CSL ITH. Wrote the paper: KJL CJH YHW SPW MPK CSL ITH.

References

1. Fahn S, Libsch L, Cutler R (1971) Monoamines in the human neostriatum: topographic distribution in normals and in Parkinson's disease and their role in akinesia, rigidity, chorea, and tremor. J Neurol Sci 14: 427–455.

2. Gilman S, Koeppe RA, Adams KM, Junck L, Kluin KJ, et al. (1998) Decreased striatal monoaminergic terminals in severe chronic alcoholism demonstrated with (+)[11C] dihydrotetrabenazine and positron emission tomography. Ann Neurol 44: 326–333.

3. Goswami R, Ponde DE, Kung MP, Hou C, Kilbourn MR, et al. (2006) Fluoroalkyl derivatives of dihydrotetrabenazine as positron emission tomography imaging agents targeting vesicular monoamine transporters. Nucl Med Biol 33: 685–694.

4. Okamura N, Villemagne VL, Drago J, Pejoska S, Dhamija RK, et al. (2010) In vivo measurement of vesicular monoamine transporter type 2 density in Parkinson disease with (18)F-AV-133. J Nucl Med 51: 223–228.

5. Lin KJ, Lin WY, Hsieh CJ, Weng YH, Wey SP, et al. (2011) Optimal scanning time window for 18F-FP-(+)-DTBZ (18F-AV-133) summed uptake measurements. Nucl Med Biol

6. Lin KJ, Weng YH, Wey SP, Hsiao I, Lu CS, et al. (2010) Whole-body biodistribution and radiation dosimetry of 18F-FP-(+)-DTBZ (18F-AV-133): a novel vesicular monoamine transporter 2 imaging agent. J Nucl Med 51: 1480–1485.

7. Braak H, Rüb U, Gai W, Del Tredici K (2003) Idiopathic Parkinson's disease: possible routes by which vulnerable neuronal types may be subject to neuroinvasion by an unknown pathogen. J Neural Transm 110: 517–536.

8. Litvan I, Paulsen JS, Mega MS, Cummings JL (1998) Neuropsychiatric assessment of patients with hyperkinetic and hypokinetic movement disorders. Arch Neurol 55: 1313.

9. Hirano S, Shinotoh H, Eidelberg D (2012) Functional brain imaging of cognitive dysfunction in Parkinson's disease. J Neurol Neurosurg Psychiatry 83: 963–969.

10. Siderowf A, Lang AE (2012) Premotor Parkinson's disease: Concepts and definitions. Movement Disorders 27: 608–616.

11. Rahman S, Griffin HJ, Quinn NP, Jahanshahi M (2008) Quality of life in Parkinson's disease: the relative importance of the symptoms. Movement Disorders 23: 1428–1434.

12. Tong J, Boileau I, Furukawa Y, Chang LJ, Wilson AA, et al. (2011) Distribution of vesicular monoamine transporter 2 protein in human brain: implications for brain imaging studies. J Cereb Blood Flow Metab 31: 2065–2075.

13. Tong J, Hornykiewicz O, Furukawa Y, Kish SJ (2007) Marked dissociation between high noradrenaline versus low noradrenaline transporter levels in human nucleus accumbens. J Neurochem 102: 1691–1702.

14. Sun J, Xu J, Cairns NJ, Perlmutter JS, Mach RH (2012) Dopamine D1, D2, D3 Receptors, Vesicular Monoamine Transporter Type-2 (VMAT2) and Dopamine Transporter (DAT) Densities in Aged Human Brain. PLOS ONE 7: e49483.

15. Tsao HH, Lin KJ, Juang JH, Skovronsky DM, Yen TC, et al. (2010) Binding characteristics of 9-fluoropropyl-(+)-dihydrotetrabenzazine (AV-133) to the vesicular monoamine transporter type 2 in rats. Nucl Med Biol 37: 413–419.

16. Mazziotta JC, Toga AW, Evans A, Fox P, Lancaster J (1995) A probabilistic atlas of the human brain: theory and rationale for its development. The International Consortium for Brain Mapping (ICBM). Neuroimage 2: 89–101.

17. Tzourio-Mazoyer N, Landeau B, Papathanassiou D, Crivello F, Etard O, et al. (2002) Automated anatomical labeling of activations in SPM using a macroscopic anatomical parcellation of the MNI MRI single-subject brain. Neuroimage 15: 273–289.

18. Oh M, Kim JS, Kim JY, Shin KH, Park SH, et al. (2012) Subregional patterns of preferential striatal dopamine transporter loss differ in Parkinson disease, progressive supranuclear palsy, and multiple-system atrophy. J Nucl Med 53: 399–406.

19. Scherman D, Raisman R, Ploska A, Agid Y (1988) [3H] Dihydrotetrabenazine, a New In Vitro Monoaminergic Probe for Human Brain. J Neurochem 50: 1131–1136.

20. Koeppe RA, Frey KA, Kuhl DE, Kilbourn MR (1999) Assessment of Extrastriatal Vesicular Monoamine Transporter Binding Site Density Using Stereoisomers of [11C] Dihydrotetrabenazine. J Cereb Blood Flow Metab 19: 1376–1384.

21. Brooks DJ, Piccini P (2006) Imaging in Parkinson's disease: the role of monoamines in behavior. Biol Psychiat 59: 908.

22. Koeppe R, Frey K, Vander Borght T, Karlamangla A, Jewett D, et al. (1996) Kinetic evaluation of [11C] dihydrotetrabenazine by dynamic PET: measurement of vesicular monoamine transporter. J Cereb Blood Flow Metab 16: 1288–1299.

23. Henry JP, Scherman D (1989) Radioligands of the vesicular monoamine transporter and their use as markers of monoamine storage vesicles. Biochemical pharmacology 38: 2395–2404.

24. McNamee RL, Yee SH, Price JC, Klunk WE, Rosario B, et al. (2009) Consideration of optimal time window for Pittsburgh compound B PET summed uptake measurements. J Nucl Med 50: 348–355.

25. Logan J, Fowler JS, Volkow ND, Wang GJ, Ding YS, et al. (1996) Distribution volume ratios without blood sampling from graphical analysis of PET data. J Cereb Blood Flow Metab 16: 834–840.

26. Weng YH, Yen TC, Chen MC, Kao PF, Tzen KY, et al. (2004) Sensitivity and specificity of 99mTc-TRODAT-1 SPECT imaging in differentiating patients with idiopathic Parkinson's disease from healthy subjects. J Nucl Med 45: 393–401.

27. Chan G, Holden JE, Stoessl AJ, Samii A, Doudet DJ, et al. (1999) Reproducibility studies with 11C-DTBZ, a monoamine vesicular transporter inhibitor in healthy human subjects. J Nucl Med 40: 283.

28. Kilbourn MR, DaSilva JN, Frey KA, Koeppe RA, Kuhl DE (1993) In vivo imaging of vesicular monoamine transporters in human brain using [11C] tetrabenazine and positron emission tomography. J Neurochem 60: 2315–2318.

29. Haycock JW, Becker L, Ang L, Furukawa Y, Hornykiewicz O, et al. (2003) Marked disparity between age-related changes in dopamine and other presynaptic dopaminergic markers in human striatum. J Neurochem 87: 574–585.

30. Troiano AR, Schulzer M, Fuente-Fernandez RL, Mak E, Mckenzie J, et al. (2010) Dopamine transporter PET in normal aging: dopamine transporter decline and its possible role in preservation of motor function. Synapse 64: 146–151.

31. Bohnen NI, Albin RL, Koeppe RA, Wernette KA, Kilbourn MR, et al. (2006) Positron emission tomography of monoaminergic vesicular binding in aging and Parkinson disease. J Cereb Blood Flow Metab 26: 1198–1212.

32. Volkow N, Fowler J, Wang G, Logan J, Schlyer D, et al. (1994) Decreased dopamine transporters with age in healthy human subjects. Ann Neurol 36: 237–239.

33. Tzen KY, Lu CS, Yen TC, Wey SP, Ting G (2001) Differential diagnosis of Parkinson's disease and vascular parkinsonism by 99mTc-TRODAT-1. J Nucl Med 42: 408–413.

34. Innis RB, van Dyck CH, Seibyl JP, Malison RT, Laruelle M, et al. (2002) Age-related decline in dopamine transporters: analysis of striatal subregions, nonlinear effects, and hemispheric asymmetries. AM J Geriat Psychiat 10: 36–43.

35. Frey KA, Koeppe RA, Kilbourn MR, Vander Borght TM, Albin RL, et al. (1996) Presynaptic monoaminergic vesicles in Parkinson's disease and normal aging. Annals of neurology 40: 873–884.

36. Kim JK, Ahn JH, Park T, Ahn HJ, Kim CS, et al. (2002) Virtual cystoscopy of the contrast material—filled bladder in patients with gross hematuria. AM J Roentgenol 179: 763–768.

37. Villablanca JP, Jahan R, Hooshi P, Lim S, Duckwiler G, et al. (2002) Detection and characterization of very small cerebral aneurysms by using 2D and 3D helical CT angiography. AM J Neuroradiol 23: 1187–1198.

38. Kim J, Cai W, Eberl S, Feng D (2007) Real-time volume rendering visualization of dual-modality PET/CT images with interactive fuzzy thresholding segmentation. IEEE T Inf Technol B 11: 161–169.